THE DRAFT ASTROPHYSCAL JOURNAL, 999:L1-L4, printed March 16, 1999

PHOTON CONSERVING RADIATIVE TRANSFER AROUND POINT SOURCES IN MULTI–DIMENSIONAL NUMERICAL COSMOLOGY

TOM ABEL[1,2], MICHAEL L. NORMAN[1,3], AND PIERO MADAU[4,5]

ABSTRACT

Many questions in physical cosmology regarding the thermal and ionization history of the intergalactic medium are now successfully studied with the help of cosmological hydrodynamical simulations. Here we present a numerical method that solves the radiative transfer around point sources within a three dimensional cartesian grid. The method is energy conserving independently of resolution: this ensures the correct propagation speeds of ionization fronts. We describe the details of the algorithm, and compute as first numerical application the ionized region surrounding a mini-quasar in a cosmological density field at $z = 7$.

Subject headings: radiative transfer — galaxies: formation — cosmology: theory — galaxies: intergalactic medium — galaxies: ISM

1. INTRODUCTION

The incorporation of radiation processes and radiative transfer into cosmological hydrodynamical simulations is essential for modeling the structure and evolution of the Ly α forest (Cen et al. 1994; Zhang, Anninos, & Norman 1995; Hernquist et al. 1996; Haehnelt & Steinmetz 1997), interpreting the observations of helium and metal line absorbers at high redshift (Reimers et al. 1997; Hellsten et al. 1997; Songaila 1998), and for simulating the early reheating and reionization of the intergalactic medium (IGM) (Ostriker & Gnedin 1996; Gnedin & Ostriker 1997). In the last case the large computational effort is justified by the hope that the study of the transition from a neutral IGM to one that is almost fully ionized could provide some hints on the first generation of stars and quasars in the universe. Until now, radiative transfer effects have either been ignored in such simulations, or treated as a self-shielding correction to an optically thin approximation (Katz et al. 1996; Gnedin & Ostriker 1997). Typically, radiation fields are treated as isotropic backgrounds $J_\nu(z)$ which are either specified as an external function computed by other means (e.g., Haardt & Madau 1996), or are computed by averaging over all sources within the computational volume (Cen 1994; Gnedin & Ostriker 1997). Only approximate treatments exist of the reprocessing of radiation via absorptions internal to the sources as well as by the IGM, an effect that can significantly influence the spectrum of the metagalactic flux (Haardt & Madau 1996). Moreover, at $z \gtrsim 3$ (5) the IGM itself is opaque in the helium (hydrogen) Lyman continuum, and radiation backgrounds become increasingly inhomogeneous and anisotropic (Reimers et al. 1997; Madau, Haardt, & Rees 1999). Recent analytic work has attempted to forge a closer connection between sources, transport, and sinks of cosmic radiation, albeit in a spatial– and angle–averaged way (Haiman & Loeb, 1998a, b; Madau, Haardt & Rees 1999).

In this paper we describe an approach to cosmological radiative transfer which relaxes these assumptions, and is appropriate on scales comparable to the separation of individual sources of radiation. Our method has the property that energy is conserved independently of numerical resolution, ensuring, for example, that ionization fronts propagate at the correct speed. The radiation driven front surrounding a mini-quasar in a cosmological density field at $z = 7$ is computed as a first application of the technique.

2. COSMOLOGICAL RADIATIVE TRANSFER

The equation of cosmological radiative transfer in comoving coordinates (cosmological, not fluid) is (Norman, Paschos & Abel 1998):

$$\frac{1}{c}\frac{\partial I_\nu}{\partial t} + \frac{\hat{n}\cdot\nabla I_\nu}{\bar{a}} - \frac{H(t)}{c}\left(\nu\frac{\partial I_\nu}{\partial \nu} - 3I_\nu\right) = \eta_\nu - \chi_\nu I_\nu \quad (1)$$

where $I_\nu \equiv I(t, \vec{x}, \hat{n}, \nu)$ is the monochromatic specific intensity of the radiation field, $\hat{n}$ is a unit vector along the direction of propagation of the ray; $H(t) \equiv \dot{a}/a$ is the (time-dependent) Hubble constant, and $\bar{a} \equiv \frac{1+z_{em}}{1+z}$ is the ratio of cosmic scale factors between photon emission at frequency ν and the present time t. Here η_ν, χ_ν, and c denote the emission coefficient, the absorption coefficient, and the speed of light, respectively. Equation (1) will be recognized as the standard equation of radiative transfer with two modifications: the denominator $\bar{a}$ in the second term, which accounts for the changes in path length along the ray due to cosmic expansion, and the third term, which accounts for cosmological redshift and dilution. In principle, one could solve equation (1) directly for the intensity at every point in $(t, \vec{x}, \hat{n}, \nu)$ space given η and χ. However

[1]Laboratory for Computational Astrophysics, NCSA, University of Illinois at Urbana/Champaign, 405 N. Mathews Ave., Urbana, IL 61801.
[2]Max-Planck-Institut für Astrophysik, Karl-Schwarzschild-Strasse 1, 85748 Garching, Germany.
[3]Astronomy Department, University of Illinois at Urbana–Champaign, Urbana.
[4]Space Telescope Science Institute, 3700 San Martin Drive, Baltimore MD 21218.
[5]Institute of Astronomy, Madingley Road, Cambridge CB3 0HA, UK.

the high dimensionality of the problem not to mention the high spatial and angular resolution needed in cosmological simulations make this approach impractical. Therefore we proceed through a sequence of well-motivated approximations which reduce the complexity to a tractable level.

Comparing the third with the second term in equation (1), the classical transfer equation (Kirchhoff 1860):

$$\frac{1}{c}\frac{\partial I_\nu}{\partial t} + \hat{n}\cdot\nabla I_\nu = \eta_\nu - \chi_\nu I_\nu \tag{2}$$

is recovered if the scale of interest, L, is much smaller than the horizon, $c/H(t)$. (Note that this is only true if $|\nu\frac{\partial I_\nu}{\partial \nu}| \leq I_\nu$; i.e., for continuum radiation. However, we can nonetheless still use eq. (2) for line transfer provided we Doppler shift the absorption cross section in χ_ν due to Hubble expansion.) In the case of constant absorption and emission coefficients the time derivative can also be dropped and one is left with the static transfer equation

$$\hat{n}\cdot\nabla I_\nu = \eta_\nu - \chi_\nu I_\nu. \tag{3}$$

This equation is also adequate for problems in which the absorption and emission coefficients change on timescales much longer than the light crossing time, L/c. This will always be the case in the volumes we will be able to simulate in the near future, and we thus adopt this approximation. At small distances from the source, however, this simplification will always break down allowing I–fronts to expand faster than the speed of light. This can be easily dealt with as we will show in the subsequent section.

An extensive literature exists on methods of solution for equation (3) (e.g., Mihalas & Mihalas 1984) depending on the symmetry of the problem and the properties of η_ν and χ_ν. A direct solution of equation (3) is impractical due to the high dimensionality of the problem. Our approach is approximate, and is based on decomposing the radiation field into point source and diffuse components: $I_\nu \equiv I_\nu^{pts} + I_\nu^{diff}$. The motivation for doing this is that whereas I_ν^{pts} is highly anisotropic, we expect I_ν^{diff} to be nearly isotropic, and accordingly we can employ the best methods taylored for each component.

Utilizing the linearity of the radiation field, we can write:

$$\begin{aligned}\hat{n}\cdot\nabla I_\nu^{diff} &= \chi_\nu(S_\nu - I_\nu^{diff}) \qquad (4)\\ \hat{n}\cdot\nabla I_\nu^{pts} &= -\chi_\nu I_\nu^{pts}, \qquad (5)\end{aligned}$$

where diffuse emission (e.g., due to recombination radiation) appears only in the transport equation for the diffuse radiation field via the source function $S_\nu \equiv \eta_\nu/\chi_\nu$. This has the advantage that equation (5) can now be solved ray by ray in a completely decoupled fashion. For $\chi_\nu(x) = const$, equation (5) has the simple analytic solution

$$I_\nu(x_1) = I_\nu(x_0)e^{-\tau} = I_\nu(x_0)\exp(-\chi_\nu(x_1 - x_0)). \tag{6}$$

In the next section we describe an efficient implementation for solving equation (5) on rays emanating from point sources within a uniform Cartesian grid. Several methods of solution for equation (5) are discussed in Norman, Paschos, & Abel (1998). Also more arguments justifying the physical basis of our approach are given there.

3. IMPLEMENTATION

Figure 1 gives the flowchart of the simple algorithm. Details of the individual computational steps are given in the following sections. For each point source in our volume, a set of radial rays quasi-uniformly distributed in solid angle are constructed. Enough rays are used such that every cell at large distances from the source is crossed by at least one ray *on average*. We are able to use fewer angles than one would naively assume by Monte Carlo sampling in angle within a radiation-matter coupling timescale. Each ray is discretized "cast" into ray segments according to how it intersects the cell boundaries. On each ray segment the intensity is attenuated according to equation (5) using an absorption coefficient appropriate to that cell. The number of absorptions in the frequency interval $\nu, \nu+d\nu$ in each ray segment inside a cell is simply related to the decrease in I_ν^{pts} along that segment. The total number of photoionizations in the cell is the sum over all ray segments crossing the cell.

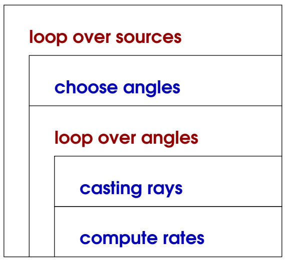

Fig. 1.— The flowchart for the radiation transfer algorithm.

3.1. *Choosing Angles*

To properly describe the I–front one needs at least $N_a = f_a \times 2\pi r/\triangle x$ rays so that at least one ray is cast to each cell of sidelength $\triangle x$ at the equator of a sphere with radius r. We introduce the factor f_a to allow us to control the number of rays. To adopt the minimum number of rays needed we store the maximum radius, r_{max}, needed to capture the furthest point of the I–front.

We use spherical coordinates (r, ϕ, θ),

$$\begin{aligned} x &= r\cos\phi\,\cos\theta, \quad 0 \leq \phi \leq 2\pi \\ y &= r\sin\phi\,\cos\theta, \quad -\frac{\pi}{2} \leq \theta \leq \frac{\pi}{2} \\ z &= r\sin\theta, \end{aligned} \tag{7}$$

and divide the sphere in segments of similar size such that all rays will have similar fluxes. We can now find the angles that define the rays which pierce through segments of roughly equal area. The discrete values for θ are given by

$$\theta_j = (j - \frac{1}{2})\frac{2\pi}{N_a} - \frac{\pi}{2}, \quad 1 \leq j \leq \frac{N_a}{2}. \tag{8}$$

Closer to the poles fewer azimuthal angles are required,

$$N_\phi^j = \max(N_a\,\cos\theta, 1). \tag{9}$$

The azimuthal angles are now chosen to be

$$\phi_i = (i - \frac{1}{2})\frac{2\pi}{N_\phi}, \quad 1 \leq i \leq N_\phi. \tag{10}$$

One also needs to know the area of the sphere segment, $A(i,j)$ described by each ray. In units of the surface of the sphere ($4\pi r^2$), this is

$$\begin{aligned} A(i,j) &= \frac{|\sin\theta_2 - \sin\theta_1|}{2N_\phi^j}, \\ \theta_1 &= (j-1)\frac{2\pi}{N_a} - \frac{\pi}{2},\ \theta_2 = j\frac{2\pi}{N_a} - \frac{\pi}{2}. \end{aligned} \quad (11)$$

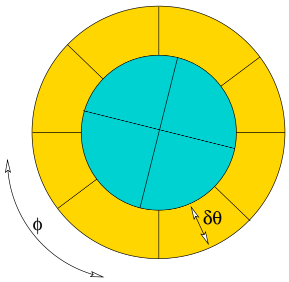

Fig. 2.— Sphere from top with the division into areas of similar size. The azimuthal angle $0 \le \phi \le 2\pi$ and $\delta\theta$ are also indicated. The varying $N_\phi(\theta)$ is evident.

A random rotation of the coordinate system is then introduced for each snapshot solution of I_ν to avoid any possible pole artifacts and reduce the number of angles required.

3.2. *Casting Rays*

Ray casting is the next step. This means to compute, for a given ray (θ,ϕ), the indices $i(l), j(l), k(l)$ of the grid cells it traverses, as well as the lengths of the ray segments $dS(l)$ within each cell. Here i,j,k are the indices of grid cells in a Cartesian lattice $x(i), y(j)$, and $z(k)$, and l is the index of the ray segment. For simplicity we restrict our discussion to uniform, isotropic grids such that $x(i) = i\Delta, y(j) = j\Delta, z(k) = k\Delta$ where Δ is the cell size and $0 \le i \le N_i$, and similarly for j and k. Ray casting is a problem in computational geometry with efficient methods discussed in books on computer graphics. For a uniform Cartesian grid the problem is straightforward. Here we write down a direct algorithm (i.e., requiring no costly sorts). Consider a point source at coordinate x_s, y_s, z_s in cell i_s, j_s, k_s. We have simply $i(1) = i_s, j(1) = j_s, k(1) = k_s$. We cast a ray in direction θ,ϕ and ask which cell boundary it intersects first. If it intersects an x boundary first, $i(2) = i(1) + \mathrm{sign}(\cos\phi), j(2) = j(1), k(2) = k(1)$, and analogously if the y or z boundaries are crossed first. To determine which cell face is crossed first, we compute the distances (radii) from the source to the next x, y or z crossings. Call these distances r_x, r_y and r_z. The minimum of these three distances determines which cell boundary is crossed first.

This can be expressed as follows: define

$$\begin{aligned} \mu &= \cos\phi, & s_\mu &\equiv \mathrm{sign}(\mu) \\ \gamma &= \sin\phi, & s_\gamma &\equiv \mathrm{sign}(\gamma) \\ \zeta &= \sin\theta, & s_\zeta &\equiv \mathrm{sign}(\zeta), \end{aligned} \quad (12)$$

then for all $l \ge 2$ we have

$$\begin{aligned} r_x(l) &= |\Delta[i(l) + \frac{1}{2}(s_\mu + 1)] - x_s| / \max(\epsilon, |\mu\cos\theta|) \\ r_y(l) &= |\Delta[j(l) + \frac{1}{2}(s_\gamma + 1)] - y_s| / \max(\epsilon, |\gamma\cos\theta|) \\ r_z(l) &= |\Delta[k(l) + \frac{1}{2}(s_\zeta + 1)] - z_s| / \max(\epsilon, |\mu\,\zeta|) \end{aligned} \quad (13)$$

$$\begin{aligned} i(l) &= i(l-1) \\ j(l) &= j(l-1) \\ k(l) &= k(l-1) \\ \text{if } [r_x(l) \le \min(r_y(l), r_z(l))] & \quad \text{then} \\ S(l) &= r_x(l) \\ i(l) &= i(l-1) + s_\mu \\ \text{if } [r_y(l) \le \min(r_x(l), r_z(l))] & \quad \text{then} \\ S(l) &= r_y(l) \\ j(l) &= j(l-1) + s_\gamma \\ \text{if } [r_z(l) \le \min(r_x(l), r_y(l))] & \quad \text{then} \\ S(l) &= r_z(l) \\ k(l) &= k(l-1) + s_\zeta. \end{aligned} \quad (14)$$

Here ϵ is a small number to avoid dividing by zero.

3.3. *Computing Rates*

Although the above technique can be applied to any absorption process, in the following we will discuss the specific case of hydrogen photoionization, and compute the photoionization rate coefficient and the associated heating term. Additional species can be treated in an analogous way. Given the path length $dS(l) = S(l) - S(l-1)$, and the absorption coefficient in cell $(i(l), j(l), k(l))$, the optical depth for photoionization along this path is given by $\tau_\nu^l = \chi_\nu[i(l), j(l), k(l)]dS(l)$. Further, from the solution of the static transfer equation (6), one sees that $\delta t \times \dot{N}_\nu(l-1)(1 - e^{-\tau_\nu^l})$ photons are absorbed in the time interval, δt. Hence, the rate of change of the neutral hydrogen density, $n_{\rm H}$, due to photoionization is simply given by,

$$\dot{n}_{\rm H} = \dot{N}_\nu^{l-1}\left[1 - e^{-\tau_\nu^l}\right] / V_{\rm cell}, \quad (15)$$

where $\dot{N}_\nu$ is the monochromatic number of photons emitted by the source per unit time, and $V_{\rm cell}$ denotes the volume of the cell. The heating rate is then,

$$\dot{e} = (h\nu - 1\,{\rm ryd})\,\dot{N}_\nu^{l-1}\left[1 - e^{-\tau_\nu^l}\right] / V_{\rm cell}. \quad (16)$$

Both of the above rates are summed over the contributions of all rays. Employing the analytical solution for each ray segment insures that I–fronts move at the correct speed independent of spatial resolution.

3.4. *Faster than light I–fronts*

In deriving equation (3) we have neglected the time dependent term of the transfer equation (1). The assumption that the light crossing time is shorter than the ionization timescale breaks down close to the source. As a consequence the I–front expands at a speed exceeding the

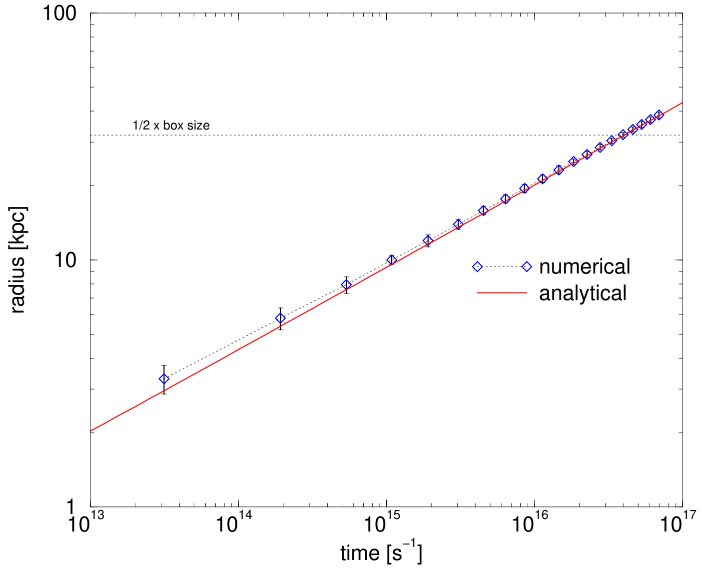

Fig. 3.— Comparison of the analytical radius of an I–front [eq. (18)] with the numerical solution on a 64^3 3D cartesian grid. The error bars indicate the maximum deviation found on the spherical ionization front. The deviations are always less than one grid cell. The straight line indicates where part of the I–front leaves the simulation volume. The cell size is 1 kpc in this test case.

speed of light. This can also be seen from the simple jump condition in a static universe,

$$4\pi r_I^2 n_{\rm H}\frac{dr_I}{dt} = \dot{N} - 4\pi\alpha_B\int_0^{r_I} n_e n_p r^2 dr, \qquad (17)$$

where α_B is the recombination coefficient to the excited states of hydrogen. In this expression, dr_I/dt exceeds the speed of light for radii less than $r_c = (\dot{N}/4\pi c n_{\rm H})^{0.5} \approx 5.3\,{\rm kpc}(\dot{N}_{56}/n_{\rm H})^{0.5}$. To avoid this unphysical effect we simply do not compute rates at distances further than $r_l = c(t - t_{\rm on})$. The radius r_l is also used in the computation of the optical depths in equations (16) and (15). Additionally, to speed up the calculation for radii $r < r_c$ we evolve the equations on a tenth of the light travel time across one cell. As a consequence the time evolution of the ionized fraction close to the source will not be computed correctly. However, we do not consider this a severe limitation since the neutral fraction becomes practically zero in regions within a light travel time from the radiation Source.

4. A TEST AND AN APPLICATION

In this section we first provide a test case that demonstrates the accuracy of the method and then, as first application, compute the ionized region surrounding a "mini-quasar" in a cosmological density field at $z = 7$. Mini-quasars could be common at early epochs if black holes can form in the first 10^8 $M_\odot$ cold dark matter (CDM) condensations (Haiman & Loeb 1998b).

4.1. *Spherical I–front Test*

To test our algorithm we set up a point source in a uniform medium, and neglect the effect of radiative recombinations. The radius of the spherically expanding I–front can be derived analytically by balancing the number of emitted photons with the hydrogen atoms that are present in the ionized volume,

$$R_I(\triangle t) = \left(\frac{3\dot{N}}{4\pi n_{\rm H}}\triangle t\right)^{\frac{1}{3}}. \qquad (18)$$

Figure 3 compares this analytical solution with the results of our algorithm on a 64^3 grid. The radius and the spherical geometry are perfectly recovered within the accuracy of the spatial resolution. The specific parameters used in this test were $\dot{N} = 10^{51}$ s^{-1}, $n_{\rm H} = 10^{-2}$ cm^{-3}, and $\triangle x = 1$ kpc. The algorithm has also been tested to reproduce accurately the size of classical Strömgren sphere in calculations where radiative recombinations are included.

4.2. *Cosmological Density Field*

Our first interesting application is the evolution of the ionization zone surrounding a mini-quasar which turns on at $z = 7$ in the inhomogeneous density field derived from cosmological simulations. The evolutionary timescale of the ionization front within our volume is $\lesssim 1$ Myr. During this time no noticeable change in the density distribution will take place on the scale of the smallest resolution element (~ 3 kpc) due to the small peculiar velocities ($< 300\,{\rm km\,s^{-1}}$). For simplicity we do not solve the energy equation and include hydrogen radiative recombinations by assuming a constant Case B recombination rate of $\alpha_B = 3.4\times10^{-13}$ cm^3 s^{-1} everywhere on The grid. This corresponds to a temperature of $\sim$ 7000 K, chosen to be rather low to enhance the effect of recombinations. For a more detailed discussion of the temperature distribution in cosmological H II regions see Abel & Haehnelt (1999).

For the background medium we use the H I distribution computed in a SCDM cosmology (with $\Omega_b = 0.06$ and $h = 0.5$) at $z = 6.941$ from Bryan et al. (1999). The 2.4 Mpc box length corresponds to 300 proper kiloparsecs. At the densest cell, which is found in a virialized halo of total mass $\approx 1.3 \times 10^{11}$ $M_\odot$, we introduce

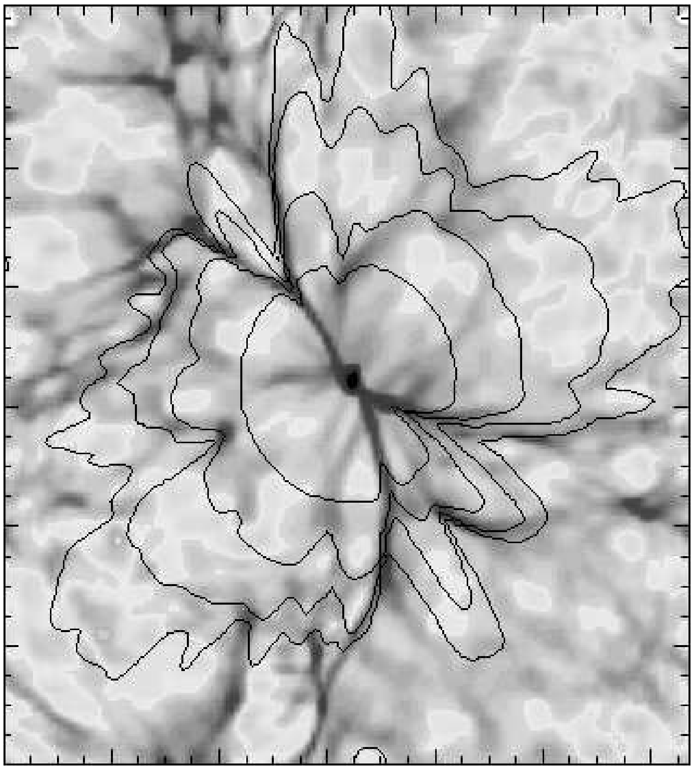

Fig. 4.— Propagation of an R-type I–front in a 128^3 cosmological density field produced by a mini-quasar with $\dot{N} = 5 \times 10^{53}$ s^{-1}. The solid contours give the position of the I–front at 0.15, 0.25, 0.38, and 0.57 Myr after the quasar has switched on. The underlying greyscale image indicates the initial H I density field.

a quasar-type source with an ionizing photon emission rate of $\dot{N} = 5 \times 10^{53}$ s^{-1}. The gas clumping factor is $\langle n_{\rm H}^2\rangle/\langle n_{\rm H}\rangle^2 = 59.2$, and is larger than the ionized hydrogen clumping factor, $C = \langle n_{\rm HII}^2\rangle/\langle n_{\rm HII}\rangle^2$, as clumps that are dense and thick enough to be self-shielded from UV radiation remain neutral and do not contribute to the recombination rate.

Figure 4 illustrates the evolution of the I–front during the first 0.6 Myr. The initial spherical expansion (at the speed of light since the number of available photons exceeds by far the number of neutral hydrogen atoms and recombinations) is quickly broken as the front expands first into the voids (increasing their thermal pressure by many orders of magnitude by photo–heating), then more slowly into the denser filaments.

In a highly inhomogeneous universe, the volume-averaged gas recombination timescale,

$$t_{\rm rec} = (n_e \alpha_B C)^{-1} = 0.1\,{\rm Gyr}\left(\frac{1+z}{8}\right)^{-3} C_{20}^{-1} \qquad (19)$$

(for $\Omega_b h^2 = 0.015$) is much shorter than the then Hubble time. At later epochs, when the size of the H II region is large compared to the scale of the clumping, the front will fill its time-varying Strömgren volume, V_S, in a few recombination times just like in the static case (Madau, Haardt, & Rees 1999),

$$V_S = \frac{\dot{N} t_{\rm rec}}{n_{\rm H}} = 0.63\,{\rm Mpc}^3 \dot{N}_{53.7}\left(\frac{1+z}{8}\right)^{-6} C_{20}^{-1}. \qquad (20)$$

This is 20 times larger than our simulation box.

5. SUMMARY

Not only for theoretical reasons, but also in light of upcoming space missions such as MAP, PLANCK, and NGST, a detailed understanding of the thermal history of the IGM and reionization is highly desirable. In this paper we have described a photon conserving algorithm which allows to simulate inhomogenous reionization self–consistently within a cosmological hydrodynamical simulation. The method employs an on-the-spot approximation to treat the effects of the diffuse emission Of ionizing photons. For scenarios in which stellar sources are responsible for the reionization of hydrogen, the on-the-spot approach is expected to give reliable results. However, for calculations in which the diffuse radiation due to helium recombinations is expected to be important a separate solver must be used. Also, if the exact topology of the ionization front needs to be captured to high accuarcy one needs to solve for the diffuse radiation separately in order not to overestimate the effect of shadowing (Norman et al. 1999). In applications where radiative recombinations can be neglected the number of rays used can be reduced significantly due to the variable choice of coordinate system for the selection of rays. Recently, a different algorithm for 3D radiative transfer in cosmological situation has been presented by Razoumov & Scott (1998). Their explicit advection scheme (at the speed of light) seems well suited for situations in which the I–fronts move faster than any hydrodynamical flow. Only temporary 2D arrays are used in the method presented here requiring negligible small additional memory for 3D cosmological hydrodynamics simulations.

Support for this work was provided by NASA through ATP grant NAG5-4236. T. A. also acknowledges support from NASA grant NAG5-3923.

REFERENCES

Abel, T., Anninos, P., Zhang, Y., & Norman, M. L. 1997a, NewA, 2, 181.
Abel, T., Anninos, P., Norman, M. L., & Zhang, Y. 1999, ApJ, in press.
Abel, T., & Haehnelt, M. G. 1999, submitted to ApJ (astro-ph/9903102)
Bryan, G. L., Machacek, M., Anninos, P., & Norman, M. L. 1999, ApJ, in press (astro-ph/9805340).
Cen, R., Miralda-Escudé, J., Ostriker, J. P., & Rauch, M. 1994, ApJ, 437.
Gnedin, N. Y., & Ostriker, J.P. 1997, ApJ, 486, 581.
Haardt, F., & Madau, P. 1996, ApJ, 461, 20.
Haehnelt, M. G., & Steinmetz, M. 1997, MNRAS, 289, L21.
Haiman, Z., & Loeb, A. 1998a, ApJ, 499, 520.
Haiman, Z., & Loeb, A. 1998b, ApJ, 503, 505.
Hellsten, U., Dave, R., Hernquist, L., Weinberg, D. H., & Katz, N. 1997, ApJ, 487, 482.
Hernquist, L., Katz, N., Weinberg, D. H., & Miralda-Escudé, J. 1996, ApJ, 457, 51L.
Katz, N., Weinberg, D. H., Hernquist, L., & Miralda-Escudé, J. 1996, ApJ, 457, 57L.
Kirchhoff, H. 1860, Phil. Mag., 19, 193.
Madau, P., Haardt, F., & Rees, M. J. 1999, ApJ, in press (astro-ph/9809058).
Mihalas, D. & Mihalas, B. 1984, *Foundations of Radiation Hydrodynamics*, New York: Oxford University Press.
Norman, M. L., Paschos, P., & Abel, T. 1998, in "H_2 in the Early Universe", eds. F. Palla, E. Corbelli, and D. Galli, (Mem. S.A.It.), 271.
Norman, M. L., Paschos, P., Abel, T., & Bordner, J. 1999, in preparation.
Ostriker, J. P., & Gnedin, N. Y. 1996, ApJ, 472, L63.
Razoumov, A. O., & Scott, D. 1998, preprint (astro-ph/9810425).
Reimers, D., Köhler,S., Wisotzki, L. Groote, D., Rodriguez-Pascual, P. & Wamsteker, W. 1997, A&A, 327, 890.
Songaila, A. 1998, ApJ, 480, L1.
Zhang, Y., Anninos, P., & Norman, M. L. 1995, ApJ, 453, L57.